J Geod (2015) 89:303–312
DOI 10.1007/s00190-014-0776-y

ORIGINAL ARTICLE

Center-of-mass corrections for sub-cm-precision laser-ranging targets: Starlette, Stella and LARES

Toshimichi Otsubo · Robert A. Sherwood · Graham M. Appleby · Reinhart Neubert

Received: 8 August 2014 / Accepted: 30 October 2014 / Published online: 13 November 2014

Abstract To realize the full potential of satellite laser ranging for accurate geodesy, it is crucial that all systematic effects in the measurements are taken into account. This paper derives new values for the so-called center-of-mass corrections for three geodetic satellites that are regularly tracked and used in geodetic studies. Optical responses of the twin satellites, Starlette and Stella, and the LARES satellite are retrieved from kHz single-photon laser-ranging data observed at Herstmonceux and Potsdam. The detection timing inside single-photon systems, C-SPAD-based systems and photomultiplier-based systems is numerically simulated, and the center-of-mass corrections are derived to be in the range of 74 to 82 mm for Starlette and Stella, and 127–135 mm for LARES. The system dependence is below 1 cm, but should not be ignored for millimeter accuracy. The long-time standard center-of-mass correction 75 mm of Starlette and Stella is revealed to be too small for the current laser-ranging stations on average, which is considered to have resulted in a non-negligible systematic error in geodetic products.

Keywords Satellite laser ranging · Optical response · Starlette · Stella · LARES

T. Otsubo (✉)
Hitotsubashi University, 2-1 Naka, Kunitachi,
Tokyo 186-8601, Japan
e-mail: t.otsubo@r.hit-u.ac.jp

R. A. Sherwood · G. M. Appleby
NERC Space Geodesy Facility, Herstmonceux Castle,
Hailsham, East Sussex BN27 1RN, UK

R. Neubert
Deutsches GeoForschungsZentrum, Telegrafenberg,
14473 Potsdam, Germany

1 Introduction

Satellite laser ranging has played a very important role in geodesy and orbital dynamics for nearly half a century since the first successful experiment in 1964. The measurement precision has been improved dramatically: state-of-the-art laser-ranging systems now yield the scatter of full-rate residuals at a few millimeters' level RMS (root mean square), and the normal-point compression procedure produces normal-point ranges of better than 1 mm precision, given a sufficient number of returns.

The temporal spread of optical pulse signals due to reflection from multiple onboard reflectors is now one of the major error sources in satellite laser ranging, and often called the satellite signature effect. The point-to-point distance between the telescope reference point of a tracking station and the center of mass of a satellite is required for precise orbital analyses, but the actual laser pulses are reflected at the retroreflectors on the surface of a satellite. The one-way distance that has to be added to the raw range observations is called the center-of-mass correction.

This error source had been recognized since the 1980s (Degnan 1985; Schwartz 1990), but it was in the early 1990s when the distribution of the residuals from full-rate data was found to depend on the satellite (Appleby 1992). As laser-ranging precision improves, the satellite signature effect has become one of the major error sources along with system hardware/procedure issues and atmospheric delay corrections. It then led to recognition that the center-of-mass correction for spherical geodetic satellites should no longer be treated as a universal constant, but as a system-dependent value (Neubert 1994). This effect was first detected in a relatively large satellite, Ajisai (Otsubo et al. 1999), and the system-dependent center-of-mass corrections were precisely studied for spherical geodetic satellites (Otsubo and Appleby

Fig. 1 Starlette (*left*) and LARES (*right*). The proportion of the scale is kept. *Left* http://wwwrc.obs-azur.fr/gemini/themes/geo/satellites/. *Right* http://www.lares-mission.com/

2003) where it was revealed that the center-of-mass correction depends on the ranging system and observation policy at stations and varies about 1 cm for LAGEOS and 5 cm for Ajisai and Etalon. However, with sub-centimeter precision achieved at most of the active laser-ranging stations, it is timely to look into even smaller spherical satellites: relatively old twin Starlette and Stella, and a new satellite LARES launched in 2012.

Starlette, shown on the left of Fig. 1, was launched by CNES (Centre National d'Etudes Spatiales), France in 1975. It is the very first of the sphere-shaped satellites which have the important advantage that ranging observations are almost independent of the orientation of the satellite. It was followed in 1993 by its twin, Stella, also launched by CNES. They orbit the Earth at the altitude of 800 km. Their small cross-section area for their mass reduces the perturbations acting on them, and precise orbit determination of these satellites has been conducted for the study of Earth gravity field and its variation (e.g., Chen et al. 2008; Matsuo et al. 2013).

LARES (LAser RElativity Satellite), also shown in Fig. 1, was launched in February, 2012, from the European Spaceport of Kourou. It is made of a sphere of high-density tungsten alloy, which reduces the area-to-mass ratio and is expected to reduce non-conservative forces to the utmost limit. Its altitude is 1,500 km. This satellite is primarily designed to enhance the measurement of fundamental physics and general relativity (Paolozzi et al. 2011; Ciufolini et al. 2013).

Given the availability of new, precise Earth gravity field models, primarily derived from the ongoing GRACE mission, those low-orbit satellites can now be used for positioning and terrestrial reference frames' determination, either in combination with or as independent verification of the solutions from the LAGEOS satellites which hitherto dominated this work.

In comparison to the two LAGEOS satellites that have a system-dependent target signature effect of about 1 cm, these small satellites have a clear advantage in terms of ranging measurement accuracy, but there have been no models established for them at the 1 mm level. The purpose of this study is to provide the precise center-of-mass corrections of the three satellites, Starlette, Stella and LARES, so as to meet mm-precision orbit determination and geodetic analysis in the future.

2 Retrieval of target response functions from single-photon kHz laser ranging

2.1 Single-photon kHz laser ranging

In orbit determination using satellite laser-ranging data, it is common to use normal-point data which represent multiple observations taken during a certain time span, typically a minute or so. However, to determine the optical response of the satellites, we need the full-rate observation data that contains all two-way observations.

The return energy is strictly controlled to one photoelectron or less at a few laser-ranging stations, such as the Natural Environment Research Council (NERC) Space Geodesy Facility, Herstmonceux, and the Potsdam station of Deutsches GeoForschungsZentrum, Germany. This operation policy, so-called single-photon ranging, can get rid of intensity-dependent errors, and is very useful for satellite signature studies, because the full-rate residual profile can reproduce the average optical response of a satellite. The return rate is controlled below 15 % during ranging by inserting and controlling an ND filter in front of the photodetector.

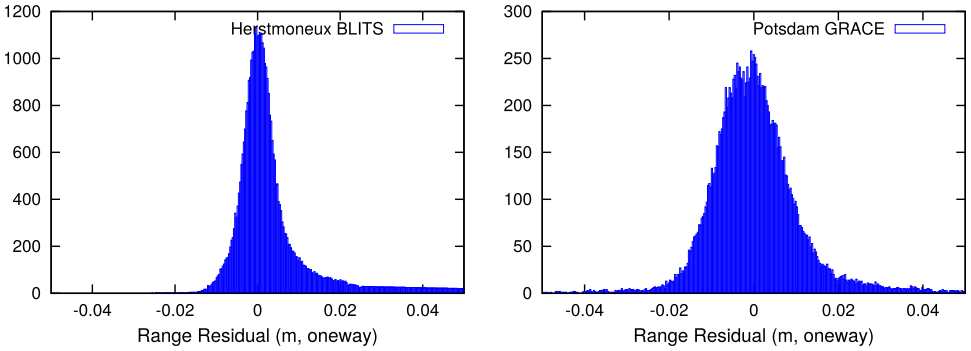

Fig. 2 The system noise profiles $S(x)$ of single-photon kHz stations. *Left* loosely edited residual histogram of BLITS laser-ranging data tracked from Herstmonceux station in October–December 2012. *Right* loosely edited residual histogram of GRACE laser-ranging data tracked from Potsdam station in April–August 2013

Although the spherical satellites are designed to be less dependent on the angle of incidence, as a satellite spins, the optical response from a whole satellite varies with a time-varying angle of incidence (Otsubo et al. 2000; Kucharski et al. 2010). A response function is then defined as an optical response averaged over all angles of incidence. If we could ignore the noise sources other than the target signature effect, the full-rate residual profile observed at a single-photon system would correspond exactly to the response function. In reality, however, we should take into account the system noise, and the full-rate residual profile is expressed as a convolved function of the system noise and the target response function.

Technical advancement in laser systems has been remarkable in the past decade. In particular, high repetition rate and short pulse width (Kirchner and Koidl 2004) are expected to greatly help the target signature studies on the condition that laser-ranging observation is operated strictly at single photon. The UK Herstmonceux station had implemented such a new laser system of 2 kHz repetition rate and 10 ps pulse width in 2006 (Gibbs et al. 2006), and has intermittently operated with it since then. In comparison to the station's conventional 14 Hz laser system, the return yield from the kHz laser is some 100 times greater for low altitude satellites, for which the laser energy is usually sufficient for a strong link budget. The Potsdam station in Germany also upgraded its laser-ranging system to 2 kHz (4 kHz at maximum) repetition and 15 ps pulse width in 2012 (Grunwaldt et al. 2013). These two stations hold an observation policy that the return energy is controlled to 0 or 1 photoelectrons. A maximum of nearly 100,000 observations have been made during a single pass of a low-orbit satellite even at such a controlled low return rate. The large number of returns enabled by the higher repetition rates leads to a much smoother profile of full-rate residuals and there is no need to accumulate a large number of passes. Further, the short pulses associated with kHz lasers and, when used in combination with high-speed detectors, lead to high precision, which will be useful to investigate the small satellite signature targets.

2.2 System noise profile

Every laser-ranging station conducts ground target ranging for calibration purpose before and after the ranging observation to a satellite, and, in the absence of satellite signature, these observations generally yield the smallest scatter. It may seem straightforward to use the ground target ranging data to represent the system noise. However, the atmosphere also is known to broaden the scatter of full-rate observations (Kral et al. 2005). Because for this study we need to retrieve the optical response of spherical satellites, let us take the atmosphere into the "system" by adopting satellite ranging data to small signature targets as the underlying system noise function.

The BLITS (Ball Lens In The Space) satellite of Russia, launched in September 2009, is made of dual spherical glasses that can retroreflect a laser pulse in a different way from a conventional corner cube-type reflector (Vasiliev et al. 2007). The single-photon laser ranging data to this satellite is ideal for constructing the profile of system noise because the satellite itself acts like a single retroreflector. It should be noted here that this innovative "zero-signature" concept has been proven successful, but it was lost in space due to a collision with debris in January 2013 (Parkhomenko et al. 2013).

The full-rate residual profile of the single-reflector BLITS satellite is plotted on the left of Fig. 2, created from a data set of 7 passes observed at Herstmonceux, approximately 35,000 single-shot observations, from October to December, 2012. The distribution is obviously asymmetric with a long tail that derives from the characteristics of a single-photon avalanche diode (SPAD). Although laser-ranging stations usually apply an iterative outlier rejection procedure by setting a clipping point at $2\times$ to $3\times$ RMS, a much looser criterion ($25\times$) RMS is specially applied for this BLITS data set so that the tail is kept. The FWHM (full width at half-maximum) of this distribution is 8 mm, and let us avoid using RMS henceforth in this paper because it largely depends on where the clipping criterion is set and how many times it is repeated. For a Gaussian distribution, the relation between the two expressions are:

$$\mathrm{FWHM} = 2\sqrt{2\log 2}\,\mathrm{RMS} \simeq 2.35\,\mathrm{RMS} \quad (1)$$

but the distribution of the actual observations is skewed and does not follow the Gaussian. The FWHM is sensitive to the peak height, and therefore we apply a 5-ps moving average to smooth the distribution profile.

It should be noted here that no return signal comes back from the BLITS satellite for 50 % of the time because a hemisphere of its surface is metallic, and that, even when, due to its spin, the satellite does face the station, the satellite was observable only in good sky conditions because the return signal is much weaker than ordinary laser-ranging targets equipped with corner cube reflectors. Given these practical constraints, it is a remarkable progress with the kHz laser-ranging technology such that a sharp but smooth function is constructed just from 7 passes.

We also examine the Potsdam station's data in a similar way. We use a 6-pass data set to the two identical GRACE satellites, from April to August 2013. The retroreflector array of GRACE consists of 4 reflectors and is the smallest among the current laser-ranging targets. Since we need a response function from a single reflector, we in advance exclude passes with double pulses or large scatter that suggest the returns are from multiple reflectors. The residual profile is shown on the right of Fig. 2 where the FWHM is 17 mm. A Hamamatsu photomultiplier H5320 was used during this period, which results in a larger scatter but with less skew.

Let us now take the profiles in Fig. 2 as representing the system noise profile of the Herstmonceux and Potsdam systems and denote them as $S(x)$ with x being a one-way range residual.

2.3 Target response function

Except for single-reflector satellites such as BLITS, a pulse retroreflected by a geodetic satellite becomes broader than the ground-transmitted laser pulse due to the reflection from multiple reflectors located at different distances from the ground station. Based on the dimension and specification of onboard reflectors, the optical responses of Starlette and LARES are numerically simulated. Note that the Stella satellite was designed to be optically identical to Starlette.

According to Arnold (1975), the retroreflectors on Starlette have a circular face 32.8 mm in diameter with a 23.3-mm height (length from the vertex to the front face). They are made of fused silica and the back faces are coated by silver. On the other hand, those of LARES, in fact similar to those of the LAGEOS satellites, have a circular face of 38.1 mm in diameter with a 27.9 mm height, and are made of fused silica with no coating on back faces (ILRS 2012). Optical response simulation of these two kinds of retroreflectors follows Otsubo and Appleby (2003), that is, to represent it by two parameters, effective reflection area a and reflectivity e as a function of the two-dimensional angle of incidence. The latter heavily depends on the back face coating: Starlette and

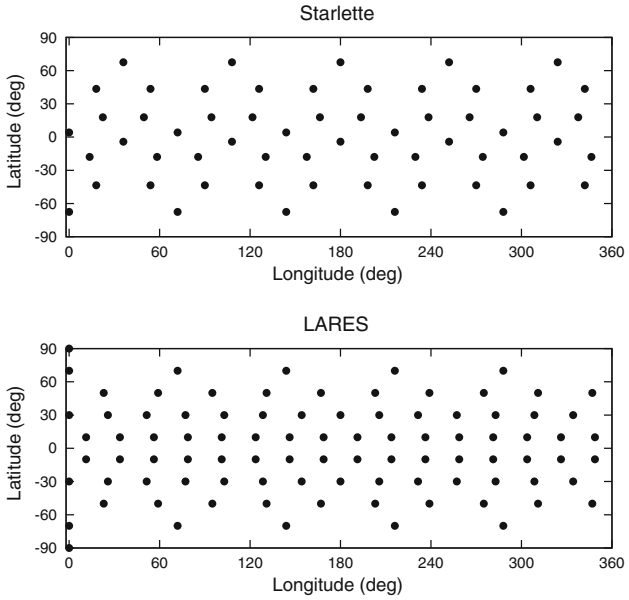

Fig. 3 Arrangement of retroreflectors installed on the surface of Starlette and Stella (*top*) and LARES (*bottom*)

Stella have a wide acceptance angle where LARES has on average a narrower acceptance angle with strong azimuthal 120° pattterns.

In theory, accurate optical simulation of each retroreflector should require only consideration of velocity abberation and there would be no need to introduce an adjusting parameter. In practice, however, the real optical behavior, i.e., far-field diffraction pattern, of a reflector is sensitive to the thermal environment in space and it is almost impossible to accurately model it. Alternatively, let us focus on statistically retrieving a satellite response function. The intensity I of a return pulse can be expressed as:

$$I \propto a^n e \tag{2}$$

with an adjusting parameter n. The intensity I is the function of two-dimensional angle of incidence.

Starlette and Stella have 60 each, and LARES has 92 retroreflectors on their spherical surfaces. The coordinates of all retroreflectors are supplied in Arnold (1975) and ILRS (2012) and are plotted in Fig. 3.

For a given angle of incidence toward a satellite, the optical response of a whole satellite can be numerically simulated by adding contributions from every retroreflector. By repeating this for more than 18,000 times, for angles at an interval of 1.5°, the average response function is built by summing the ones of all cases. We construct the average response functions of the satellites assuming n from 0.6 to 2.0 with a step size of 0.1. Among them, three cases of $n = 0.8$, 1.3, and 1.8 are plotted in Fig. 4. We denote a satellite response function as $R(x)$.

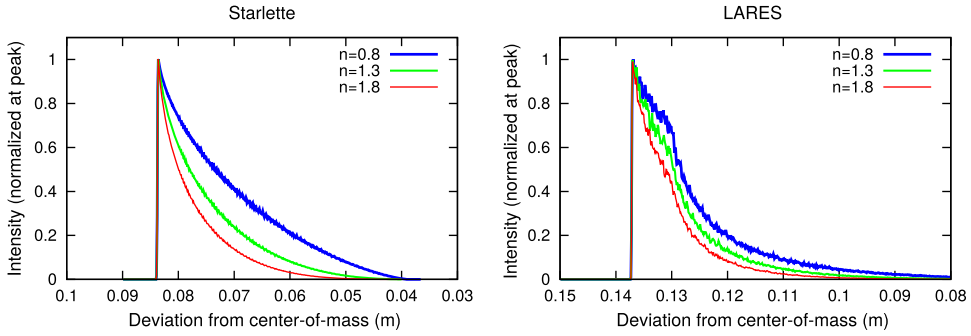

Fig. 4 Target response functions $R(x)$ of Starlette and Stella (*left*) and LARES (*right*) for three n values

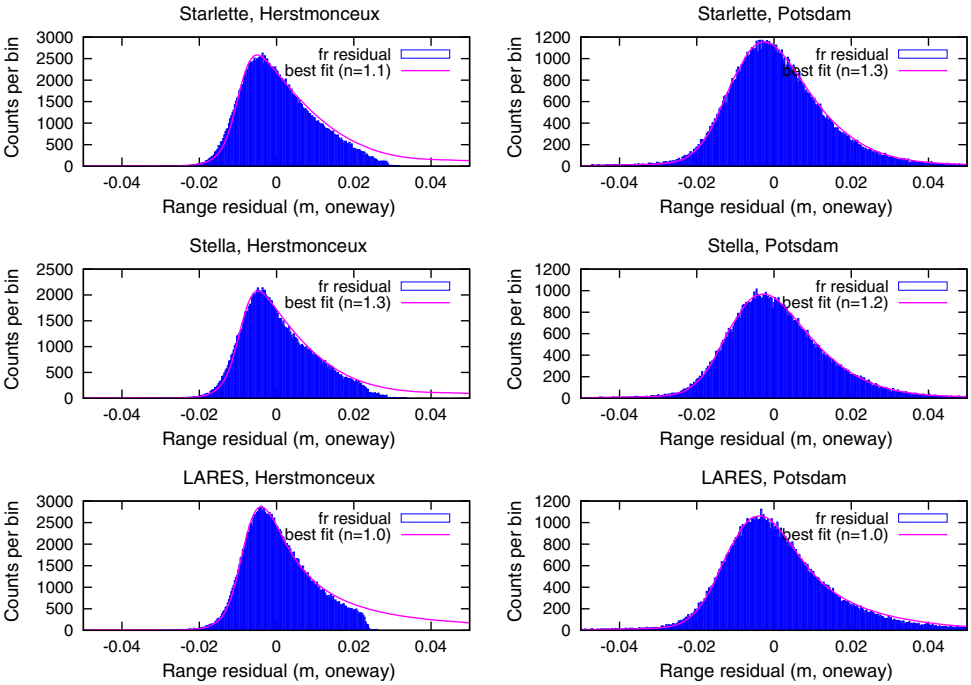

Fig. 5 Full-rate residual profiles $T_{\mathrm{obs}}(x)$ (*blue*) and the best-fit convolved function T_{n_i} (*pink*)

2.4 Search for the best-fit functions

Full-rate residual histograms of single-photon laser-ranging data are useful to determine the best-fit value for the floating parameter n. Under an unrealistically ideal condition that there were no velocity aberration and the far-field diffraction pattern followed the Airy disc, the parameter would be equal to 2. In reality, however, it is much smaller than 2. The optical design would be poorly optimized if the intensity were well below proportional ($n = 1$) to the effective reflection area. Note that the previous study had obtained values of n in the range of 1.1 to 1.3 when the same procedure was applied to LAGEOS, Ajisai and Etalon (Otsubo and Appleby 2003).

As shown in Fig. 5, also for the smaller satellites like Starlette, Stella, and LARES, the full-rate residuals scatter more than system noise profiles $S(x)$ in Fig. 2. Let us now denote them as $T_{\mathrm{obs}}(x)$. The time period of these observations are almost the same as those of the system noise $S(x)$ for both stations. The scatter is clearly larger than the system noise. This is due to the target signature, and the broadening of the Starlette–Stella twin is comparable in magnitude to that of LARES. It amounts to 15–16 mm for Herstmonceux, and 22–23 mm for Potsdam, both in FWHM. Unlike the BLITS data set, we use the Herstmonceux data whose tail is already filtered on site. On the other hand, Potsdam data keep the whole profile. This does not influence the result, because the tail regions, below 15 % of the peak, are excluded when a function is fitted as described later in this section.

In theory, the full-rate residual histogram can be written as a convolution of a system noise profile and a target response function.

$$T_{n_i}(x) = S(x) * R_{n_i}(x) \tag{3}$$

The subscript n_i indicates one of the n values with which we have computed the target response functions in Sect. 2.3. The actual observations $T_{\mathrm{obs}}(x)$ are now used to find the best-fit n values.

By forming the cumulative distribution functions, the Kolmogorov–Smirnov statistic is adopted as a indicator to be minimized by adjusting two parameters, the scale in the

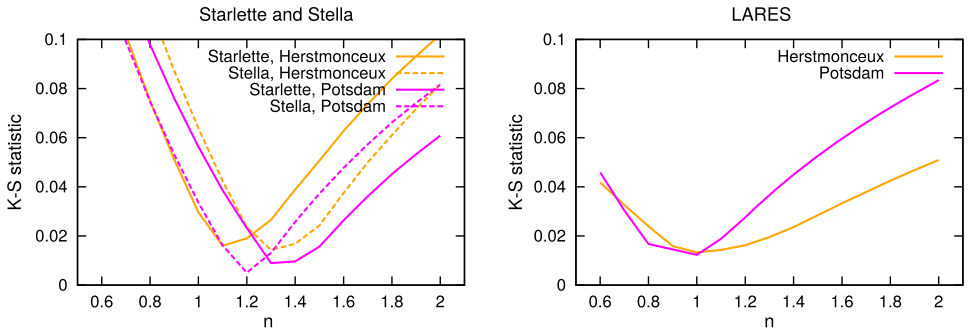

Fig. 6 The minimized Kolmogorov–Smirnov statistic for the two functions $T_{n_i}(x)$ and $T_{\mathrm{obs}}(x)$. *Left* Starlette and Stella. *Right* LARES

vertical axis and the relative shift along the horizontal axis. This is repeated for n ranging from 0.6 to 2.0, and the result is plotted in Fig. 6.

In the left graph of Fig. 6, there are four cases (two stations and two satellites), and the best-fit n value always falls between 1.1 and 1.3 as shown in Fig. 5. Note that the impact on the center-of-mass correction is smaller than 1 mm even if the parameter n changes by 0.3, and therefore the agreement here corresponds to the center-of-mass correction accuracy much better than 1 mm. We also confirm that, as expected, there is no significant difference in optical response between the twins, and let us take $n = 1.2$ for Starlette and Stella. As shown in the right graph, the best-fit function is found at 1.0 for LARES in the results from both stations. Now we obtain:

$$n = 1.2 \text{ (Starlette and Stella)} \quad (4)$$

$$n = 1.0 \qquad \text{(LARES)} \quad (5)$$

and let us take the optical response functions defined by these n values in the following section.

3 Center-of-mass corrections

The center-of-mass correction is the one-way distance to be added to the range observation so that it effectively reaches the center of mass of a satellite. We simulate the optical signal not only of a satellite with the actual optical configuration but also of an imaginary zero-size target located at the satellite's center of mass. The difference between the two signals is the center-of-mass correction.

3.1 Single-photon system

As discussed in the previous section, the single-photon observation policy adopted in Herstmonceux and Potsdam makes it possible to retrieve the average profile of a target optical response, and the center-of-mass correction should be defined at the centroid of the distribution.

First, let us look at the "1 ps" case when the system noise is practically negligible. The centroid of an optical response function corresponds to the center-of-mass correction. With the values of n as obtained in the previous section, it falls at 75 mm for Starlette and Stella and 127 mm for LARES (Table 1).

Table 1 Center-of-mass corrections for single-photon stations (unit: mm)

	Starlettte and Stella	LARES
1 ps FWHM		
No clipping	75	127
Iterative 3.0-sigma clipping	75	129
Iterative 2.5-sigma clipping	76	131
Iterative 2.0-sigma clipping	78	133
30 ps FWHM		
No clipping	75	127
Iterative 3.0-sigma clipping	75	129
Iterative 2.5-sigma clipping	76	130
Iterative 2.0-sigma clipping	78	132
100 ps FWHM		
No clipping	75	127
Iterative 3.0-sigma clipping	75	128
Iterative 2.5-sigma clipping	75	129
Iterative 2.0-sigma clipping	77	130
300 ps FWHM		
No clipping	75	127
Iterative 3.0-sigma clipping	75	127
Iterative 2.5-sigma clipping	75	128
Iterative 2.0-sigma clipping	75	128
1 ns FWHM		
No clipping	75	127
Iterative 3.0-sigma clipping	75	127
Iterative 2.5-sigma clipping	75	127
Iterative 2.0-sigma clipping	75	127
Herstmonceux		
Iterative 3.0-sigma clipping after Gaussian fit	74	127
Potsdam		
Iterative 2.5-sigma clipping	75	130

When a set of normal points is generated at a laser-ranging station, an iterative noise rejection procedure is applied to reject outliers at a rejection criteria of 2× to 3× RMS. As the residual distribution is skewed due to the target response function and also due to the characteristics of an avalanche

photodiode, the tail of a distribution is trimmed to a certain level even though it is a part of a satellite's response. The mean accordingly shifts toward the leading edge, and therefore the center-of-mass correction depends on the clipping criteria.

Now move down to the cases with system noise, 30–1,000 ps FWHM, in Table 1. The response function is convolved with various widths of Gaussian distribution which simplistically models not only a laser pulse width, but also an effect of the atmosphere, a response jitter of the detector, a jitter of the timing system, and pulse decay in cables.

The LARES satellite has a response function with more skewness than Starlette and Stella (Fig. 4), which means that its center-of-mass correction is more sensitive to the outlier rejection criteria.

In both types of satellites, when the clipping criteria is set loose (e.g., at 3× RMS), it is relatively consistent with different pulse widths. As it gets tighter (e.g., at 2× RMS), the center-of-mass correction becomes more dependent on the pulse width.

The real system noise profiles in Fig. 2 can be used for Herstmonceux and Potsdam instead of the above simplified system noise with Gaussian distribution. The skewness in the system noise profile, most pronounced in the Herstmonceux case, moves the effective reflection point closer to the satellite center because the long tail partly survives in the function convolved with a target response function. In addition, a minor detail in the data reduction process is simulated: Herstmonceux station applies a 3-sigma clipping where the mean and the sigma are defined by the best-fit Gaussian function instead of the ordinary standard deviation. The center-of-mass corrections for the two stations are specifically given at the bottom of Table 1.

Table 2 Center-of-mass corrections for C-SPAD stations (unit: mm)

	Starlettte and Stella	LARES
1 ps FWHM		
No clipping	75/77/82/82	127/130/135/135
Iterative 3.0-sigma clipping	75/78/82/82	129/132/135/135
Iterative 2.5-sigma clipping	76/79/82/82	131/133/135/135
Iterative 2.0-sigma clipping	79/81/82/82	133/134/135/135
30 ps FWHM		
No clipping	75/76/80/81	127/129/134/134
Iterative 3.0-sigma clipping	75/77/80/81	129/131/134/134
Iterative 2.5-sigma clipping	76/78/81/81	130/132/134/134
Iterative 2.0-sigma clipping	78/80/81/81	132/133/134/134
100 ps FWHM		
No clipping	75/75/79/80	127/128/130/133
Iterative 3.0-sigma clipping	75/76/79/79	128/129/132/133
Iterative 2.5-sigma clipping	75/76/79/79	129/130/132/133
Iterative 2.0-sigma clipping	77/78/78/79	130/131/132/133
300 ps FWHM		
No clipping	75/75/76/77	127/128/130/131
Iterative 3.0-sigma clipping	75/75/76/77	127/128/130/131
Iterative 2.5-sigma clipping	75/75/76/77	128/129/130/130
Iterative 2.0-sigma clipping	75/76/76/76	128/130/130/130
1 ns FWHM		
No clipping	75/75/75/75	127/127/128/128
Iterative 3.0-sigma clipping	75/75/75/75	127/128/128/128
Iterative 2.5-sigma clipping	75/75/75/75	127/128/128/128
Iterative 2.0-sigma clipping	75/75/75/75	127/128/128/128

Four numbers separated by slashes are the values when the detection energy is at 0.1, 1, 10 and 100 photoelectrons

3.2 C-SPAD system

Unlike Herstmonceux station, there are also a number of stations using a SPAD detector without strictly controlling the return energy, that is, their detection level can vary from one to many photoelectrons.

A SPAD detector introduces time walk effects as a function of the return energy. It is nowadays common to compensate it with an additional circuit and such a detector system is known as C-SPAD (Compensated-SPAD; Kirchner et al. 1998). The compensation electronics can be built from laser-ranging tests to a terrestrial target that does not broaden the laser pulse. However, during satellite ranging, the signature effect broadens the return pulse, and therefore the C-SPAD cannot fully compensate for varying energy (Appleby 1996).

We now look into the intensity dependence for both types of satellites. A numerical simulation should be carried out with the satellite response functions obtained in the previous section. We do not model the detector's time walk itself in this study, but assume a simplified model that the detector responds to the first photoelectron. For a range of average numbers of photoelectrons, from 0.1 to 100, we numerically simulated the arrival time of the first photon using Poisson statistics (Neubert 1994). The same procedure is also applied to the imaginary target at the center of mass to model the C-SPAD's response.

In both cases, the stronger the signal is, the closer to the station the detection timing goes. However, the detection timing of a broadened satellite response is more sensitive than that of a transmitted short pulse. As a result, a C-SPAD cannot fully compensate the intensity dependence.

The result is listed in Table 2.

Let us start with the 0.1 photoelectron cases, the first of the four numbers, in the table. The values for 0.01 photoelectrons are not listed here but always agree with the 0.1 photoelectron case within 0.1 mm. The numbers agree with the single-photon case, and this is where the center-of-mass correction values are minimized.

Now let us look at the full range of energy levels, from 0.1 to 100 photoelectrons. Similar to the single-photon case, the center-of-mass correction stays almost at the centroid when a broad pulse is assumed. The most important issue here is that the intensity-dependent bias is clearly predicted with a short pulse, and it amounts to 6–7 mm. The critical region in terms of such a systematic bias is therefore 0.1 to 10 photoelectrons. The range observation would be stable if a station would keep the return energy always lower than 0.1 or always higher than 10 photoelectrons.

The maximum center-of-mass corrections in Table 2 are 82 mm for Starlette and Stella and 135 mm for LARES in the cases of "1 ps" system noise. It should be noted here that these are the values averaged over every two-dimensional angle of incidence. The center-of-mass correction can reach 84 mm for Starlette and Stella and 137 mm for LARES where the leading edges in Fig. 4 are located. This is the point when one of the retroreflectors lie in the straight line joining a ground station and a satellite's center of mass. However, as the satellite rotates, the retroreflector deviates from this line and the first reflection point moves farther from the station. The center-of-mass correction for the closest retroreflector varies within a range of 80–84 mm for Starlette and Stella, and 132–137 mm for LARES. Even though the satellites have slow spin rates (Kucharski et al. 2014a, b), it is unlikely that this effect will lead to systematic effects in the geodetic results since orbital solutions always use observations from many passes and this variation will average out.

The detection energy tends to be reduced at low elevation angles due to atmospheric attenuation and the long range when a station does not control the signal strength. Such an elevation-dependent bias is likely to cause a systematic error in geodetic products, and thus the stations are requested to avoid the critical energy level.

With a broad pulse such as 300 ps or 1 ns, the center-of-mass value almost equals the centroid without clipping. This is because the broad pulse masks the skewness of the target response functions. The noise clipping criteria affects the center-of-mass correction more with a shorter pulse because the convolved distribution is more skewed.

3.3 Leading edge detection in a photomultiplier system

Currently, about half of active laser-ranging stations use a photomultiplier type detector, and most of them operate at multiple-photon level for low-orbit satellites.

A return signal goes through a detector, a constant-fraction discriminator, and cables, etc., before entering a timing device. As it is difficult to precisely model the shape of a pulse, and as it varies for different stations, we instead apply a simple Gaussian noise profile and define the half-maximum point at the leading edge to be the detection timing.

Table 3 Center-of-mass corrections for photomultiplier stations (unit: mm)

	Starlettte and Stella	LARES
1 ps FWHM	82	135
10 ps FWHM	82	135
30 ps FWHM	81	135
100 ps FWHM	80	133
300 ps FWHM	77	130
1 ns FWHM	75	128

Changing the pulse width from 1 ps to 1 ns FWHM, the signal is convolved with an orientation-dependent target response function, and also with the imaginary point target at the satellite's center of mass. The center-of-mass correction is defined as the difference between the half-maximum points of these two signals and listed in Table 3.

It can be said again that the center-of-mass correction falls at the centroid when a broad pulse is assumed, and that it shifts toward the leading edge with a short pulse. Like the high energy C-SPAD case, the center-of-mass correction reaches a maximum of 82 mm for Starlette and Stella, and 135 mm for LARES. We assume a multiple-photon return always with sufficient energy in this computation, but the center-of-mass correction can be close to the centroid values as we saw for the Potsdam single-photon system.

The signal of each pulse is skewed, but the distribution of the orientation-dependent center-of-mass corrections has little skewness. As a result, the center-of-mass correction in Table 3 computed for a 3-sigma rejection does not change more than 0.2 mm with a different clipping criteria.

3.4 Discussions

Starlette and Stella are smaller than LARES in size, approximately two-thirds. However, due to the different optical response of coated and uncoated reflectors, the target signature effects of these satellites are comparable.

The ILRS has provisionally adopted 133 mm for the LARES center-of-mass correction, which was based on the assumption that its reflectors behave like LAGEOS ($n = 1.2$). This study has proved that this is a good prediction as a whole, but the systematic difference can reach 8 mm peak to peak. The centroid value of 127 mm of the LARES response function is in agreement with an independent study (Arnold 2013) that derived a centroid value of 128 mm with a 1-mm uncertainty.

For many decades, following Arnold (1975), the laser-ranging community has adopted the standard center-of-mass correction of 75 mm for Starlette and Stella. This value, defined at the centroid, had been universally valid in 1970s and 1980s since the laser-ranging precision was less than

the target signature effect. It is still valid today for single-photon systems and also for photomultiplier systems with a broad laser pulse or a slow detector response, but it has been revealed in this study that this is too small for C-SPAD systems at multiphoton detection mode and photomultiplier systems with a short laser pulse and a fast detector response. Considering the fact that the majority of the currently active laser-ranging stations are in the latter group at least when they track low-orbit satellites, the center-of-mass correction of the twin satellites should have been 3–4 mm, on average, larger than 75 mm for the whole laser-ranging network.

A simple numerical simulation of a two-satellite-combined analysis of Starlette and Stella shows that a 3-mm bias in their center-of-mass corrections will map to a 1.7-ppb error of GM, and a 0.5-ppb error in the scale of a terrestrial reference frame. It is more common to combine a number of satellites for these purposes, and therefore the impact should be in general smaller.

This has been also pointed out by Ries (2008) and Sosnica et al. (2014) who estimated the center-of-mass correction of Starlette and Stella at 78 mm through precise orbit determination. This study supports both the Ries (2008) and the Sosnica et al. (2014) results independently from a different aspect, and furthermore, demonstrates that 1 mm precision cannot be attained without considering the system-dependent center-of-mass correction.

4 Conclusions

We have investigated the laser optical response of three satellites: Starlette, Stella and LARES. Unlike other spherical satellites like LAGEOS, Etalon and Ajisai, the target signature effect is below 1 cm, and therefore a constant center-of-mass correction has hitherto been adopted in orbit determination. The recent advance of kHz laser ranging technology, combined with the single-photon ranging policy, makes it possible to look into the target signature effect of these satellites.

The optical response functions are empirically retrieved using the kHz single-photon laser-ranging data observed at Herstmonceux and Potsdam. The outcomes from these two independent stations agree very well. The twin Starlette and Stella and the LARES satellites are found to have almost the same magnitude of signature effects.

We have numerically simulated the detection timing by simplistically modeling SPAD-based systems and photomultiplier-based systems, and obtained center-of-mass corrections in the range of 74–82 mm for Starlette and Stella, and 127–135 mm for LARES. This result indicates that the system dependence of the center-of-mass correction cannot be ignored if we wish to receive the full benefit of sub-cm precision.

The standard value of 75 mm has been used historically for Starlette and Stella, but it is close to the minimum of the possible range for currently active stations. The resulting 3–4 mm bias, on the global average, is considered to have mapped into any geodetic products that use these satellites.

Lastly, it should be noted that such a sub-cm treatment takes effect only when other potential sources of real systematic bias are controlled to a similar or better level at the laser ranging stations, and that analysts have to consider in detail the station configurations before adopting the center-of-mass correction values provided in this study.

Acknowledgments This work was supported by JSPS KAKENHI Grant Number 26400449.

References

Appleby GM (1992) Satellite signatures in SLR observations. In: Proceedings of 8th international workshop on laser ranging instrumentation, pp 2.1–2.14

Appleby GM (1996) Satellite laser ranging and the Etalon geodetic satellite. Ph.D. Thesis, The University of Aston in Birmingham, UK

Arnold DA (1975) Optical transfer function of Starlette retroreflector array. Technical Report RTOP 161–06-02, Smithsonian Astrophysical Observatory

Arnold DA (2013) Preliminary transfer function of the LARES satellite. In: Proceedings of 18th international workshop on laser ranging, 13-0408

Chen JL, Wilson CR (2008) Low degree gravity changes from GRACE, Earth rotation, geophysical models, and satellite laser ranging. J Geophys Res 113:B06402

Ciufolini I, Paolozzi A, Koenig R, Pavlis EC, Ries J, Matzner R, Gurzadyan V, Penrose R, Sindoni G, Paris C (2013) Fundamental physics and general relativity with the LARES and LAGEOS satellites. Nucl Phys B 243–244:180–193

Degnan JJ (1985) Satellite laser ranging: current status and future prospects. IEEE Trans Geosci Remote Sens GE-23(4):398–413

Gibbs P, Potter C, Sherwood RA, Wilkinson M, Benham D, Smith V, Appleby GM (2006) Some early results of kilohertz laser ranging at Herstmonceux. In: Proceedings of 15th international workshop on laser ranging, pp 250–258

Grunwaldt L, Weisheit S, Steinborn J (2013) Upgrade of SLR Station 7841 Potsdam. In: Proceedings of 18th international workshop on laser ranging, 13-Po56

ILRS (2012) Mission LARES. http://ilrs.gsfc.nasa.gov/missions/satellite_missions/current_missions/lars_general.html

Kirchner G, Koidl F (2004) Graz KHz SLR system: design, experiences and results. In: Proceedings of 14th international workshop on laser ranging, pp 501–506

Kirchner G, Koidl F, Prochazka I, Hamal K (1998) SPAD time walk compensation and return energy dependent ranging. In: Proceedings of the 11th international workshop on laser ranging instrumentation, pp 245–249

Kral L, Prochazka I, Hamal K (2005) Optical signal path delay fluctuations caused by atmospheric turbulence. Opt Lett 30(14):1767–1769

Kucharski D, Otsubo T, Kirchner G, Koidl F (2010) Spin axis orientation of AJISAI determined from Graz 2 kHz SLR data. Adv Space Res 46(3):251–256

Kucharski D, Lim H-C, Kirchner G, Koidl F (2014a) Spin parameters of low Earth orbiting satellites Larets and Stella determined from satellite laser ranging data. Adv Space Res 53(1):90–96

Kucharski D, Lim H-C, Kirchner G, Otsubo T, Bianco G, Hwang J-Y (2014b) Spin axis precession of LARES measured by satellite laser ranging. IEEE Geosci Remote Sens Lett 11(3):646–650

Matsuo K, Chao BF, Otsubo T, Heki K (2013) Accelerated ice mass depletion revealed by low-degree gravity field from satellite laser ranging: Greenland, 1991–2011. Geophys Res Lett 40(17):4662–4667

Neubert R (1994) An analytical model of satellite signature effects. In: Proceedings of 9th international workshop on laser ranging instrumentation, pp 82–91

Otsubo T, Amagai J, Kunimori H (1999) The center-of-mass correction of the geodetic satellite AJISAI for single-photon laser ranging. IEEE Trans Geosci Remote Sens 37(4):2011–2018

Otsubo T, Amagai J, Kunimori H, Elphick M (2000) Spin motion of the AJISAI satellite derived from spectral analysis of laser ranging data. IEEE Trans Geosci Remote Sens 38(3):1417–1424

Otsubo T, Appleby GM (2003) System-dependent center-of-mass correction for spherical geodetic satellites. J Geophys Res 109(B4):9.1–9.10

Paolozzi A, Ciufolini I, Vendittozzi C (2011) Engineering and scientific aspects of LARES satellite. Acta Astronaut 69(3):127–134

Parkhomenko N, Shargorodsky VD, Vasiliev VP, Yurasov V (2013) Accident in orbit. In: Proceedings of 18th international workshop on laser ranging, 13-Po03

Ries J (2008) SLR bias/CoM offset issues, impact on the TRF scale. GGOS Ground Networks and Communications Working Group Meeting, Vienna. ftp://cddis.gsfc.nasa.gov/misc/ggos/0804/GNCWG_Ries_slrbias_080416

Schwartz JA (1990) Laser ranging error budget for the TOPEX/POSEIDON satellite. Appl Opt 29(25):3590–3596

Sosnica K, Jaeggi A, Thaller D, Beutler G, Dach R (2014) Contribution of Starlette, Stella, and AJISAI to the SLR-derived global reference frame. J Geod 88:789–804

Vasiliev VP, Shargorodsky VD, Novikov SB, Chubykin AA, Parkhomenko NN, Sadovnikov MA (2007) Progress in laser systems for precision ranging, angle measurements, photometry, and data transfer. ILRS Fall 2007 workshop